Verification of the SPEC code in stellarator geometries

J. Loizu[1], S. R. Hudson[2], and C. Nührenberg[1]

[1] *Max-Planck-Institut für Plasmaphysik, D-17491 Greifswald, Germany*
[2] *Princeton Plasma Physics Laboratory, PO Box 451, Princeton NJ 08543, USA*
(Dated: October 22, 2016)

We present the first calculations performed with the Stepped-Pressure Equilibrium Code (SPEC) in stellarator geometry. Provided a boundary magnetic surface, stellarator vacuum fields with islands are computed and verified to machine precision, for both a classical $l = 2$ stellarator field and for a Wendelstein 7-X limiter configuration of the first experimental campaign. Beyond verification, a detailed comparison of SPEC solutions to Biot-Savart solutions for the corresponding coil currents is shown. The level of agreement is quantified and the error is shown to be dominated by the accuracy with which the boundary representation is given. Finally, partially relaxed stellarator equilibria are computed with SPEC and verification is presented with force-balance down to machine precision.

I. INTRODUCTION

Verification and validation of numerical codes are the two milestones in the path towards predictive capability and are essential to guarantee code reliability [1]. Verification answers the question: *are we solving the equations correctly?* Validation answers the question: *are we solving the correct equations?* More precisely, code verification provides numerical proof that the code is actually solving the equations that it claims to be solving, with increasing accuracy as the numerical resolution is increased. Code validation quantifies the level of agreement between numerical predictions and experimental measurements for a given set of observables.

Fusion research increasingly depends upon fast, robust, and reliable numerical codes capable of describing three-dimensional magnetohydrodynamic (MHD) equilibria in toroidally confined plasmas, which generally consist of an intricate combination of magnetic surfaces, magnetic islands, and magnetic field-line chaos [2]. The Stepped-Pressure Equilibrium Code (SPEC) was developed as one possible approach to fulfil this highly non-trivial task [3]. SPEC has been verified in axisymmetry and for slightly perturbed configurations [3–6]. Here we present the first SPEC calculations of equilibria in stellarator geometries, including a Wendelstein 7-X (W7-X) vacuum field limiter configuration of the first experimental campaign [7].

Section II briefly describes the SPEC code. Verification of vacuum fields is presented in Sec. III, and in Sec. IV a detailed comparison of SPEC solutions to Biot-Savart solutions is presented. Section V provides a verification of stellarator equilibria with two relaxed volumes. Conclusions follow in Sec. VI.

II. THE SPEC CODE

SPEC [3] was developed to calculate MHD equilibria as extrema of the multi-region, relaxed MHD (MRxMHD) energy functional proposed by Hole, Hudson and Dewar [8, 9]. While in ideal MHD the magnetic topology is

continuously constrained, in MRxMHD the topology is only *discretely* constrained, thus allowing for partial relaxation. More precisely, the plasma is partitioned into a finite number, N, of nested volumes, V_v, that undergo Taylor relaxation. These volumes are separated by $N-1$ interfaces, I_v, that are constrained to remain magnetic surfaces during the energy minimization process. The location and shape of these surfaces is a priori unknown and determined self-consistently by a force-balance condition. MRxMHD equilibrium states satisfy

$$\nabla \times \mathbf{B} = \mu_v \mathbf{B} \quad \text{in } V_v \qquad (1)$$

$$\left[\left[p + \frac{B^2}{2}\right]\right]_v = 0 \qquad \text{in } I_v \qquad (2)$$

for $v = 1, \ldots N$, and where $[[\cdot]]_v$ is the jump across the vth interface and p is the pressure, which is constant in each relaxed volume. This class of equilibria bridges the gap between Taylor relaxed states and ideal MHD equilibrium states in a very precise way [10]. Moreover, it allows for the possibility of non-smooth solutions, which are ubiquitous to the three-dimensional MHD problem.

As of now, SPEC is a fixed-boundary code and requires specification of the boundary in terms of the harmonics of its geometry. For stellarator symmetry, a general surface can be represented as $R(\theta, \varphi)\hat{R} + Z(\theta, \varphi)\hat{Z}$, with

$$R = \sum_{mn} R_{mn} \cos\left(m\theta - nN_p\varphi\right) \qquad (3)$$

$$Z = \sum_{mn} Z_{mn} \sin\left(m\theta - nN_p\varphi\right) \qquad (4)$$

where N_p is the field periodicity and $\theta, \varphi \in [0, 2\pi]$. Here $\hat{R} = \cos\varphi\hat{i} + \sin\varphi\hat{j}$ and $\hat{Z} = \hat{k}$, where $\hat{i}$, $\hat{j}$, and $\hat{k}$ are the Cartesian unit vectors. While the boundary harmonics are given as input, the harmonics of each internal interface are unknown and iteratively adjusted during the energy minimization process in order to satisfy Eq. (2).

Akin to other equilibrium codes, SPEC also needs specification of two profiles, e.g., the pressure in each relaxed volume, $p(\psi_v)$, and the rotational transform on either side of each interface, $\iota^{\pm}(\psi_v)$, in terms of the toroidal

magnetic flux, ψ_v, enclosed by each volume. Instead of the rotational transform, it is also possible to specify the Beltrami parameter, μ_v, and the poloidal magnetic flux, $\psi_{p,v}$, enclosed by each volume; except for the innermost volume, where, as in Taylor's theory [11], only the Beltrami parameter needs to be specified in addition to the enclosed toroidal flux.

The SPEC code provides the equilibrium solution in terms of the magnetic vector potential, $\mathbf{A}$, which is written as $\mathbf{A} = A_\theta \nabla\theta + A_\varphi \nabla\varphi$ by a proper choice of gauge. In each volume, the covariant components of the vector potential are represented as

$$A_\theta(s,\theta,\varphi) = \sum_{m,n,l} A_{\theta,m,n,l} T_l(s) \cos(m\theta - nN_P\varphi) \quad (5)$$

$$A_\varphi(s,\theta,\varphi) = \sum_{m,n,l} A_{\varphi,m,n,l} T_l(s) \cos(m\theta - nN_P\varphi) \quad (6)$$

where $s \in [-1,1]$ and the toroidal coordinates (s,θ,φ) are adapted to the interface geometries defining each volume. The boundary conditions on $\mathbf{A}$ are such that the enclosed poloidal and toroidal magnetic fluxes are enforced and $\mathbf{B} \cdot \mathbf{n} = 0$ is guaranteed on the two interfaces defining the volume. The functions $T_l(s)$ are the Chebyschev polynomials of order l [12]. The numerical resolution in SPEC is therefore given by $L_{rad} \equiv \max(l)$, $M_{pol} \equiv \max(m)$, and $N_{tor} \equiv \max(n)$. We note that while M_{pol} and N_{tor} are the same in each volume, L_{rad} may be different in each volume. Finally, in the innermost volume, regularization factors are included in Eqs. (5) and (6) in order to ensure well-behaved solutions (for more details, see Ref. [3]).

III. VERIFICATION OF VACUUM FIELDS

There is a unique magnetic field $\mathbf{B}$ [13], up to a scale factor, that satisfies

$$\nabla \times \mathbf{B} = 0 \ \text{ in } V \quad (7)$$
$$\nabla \cdot \mathbf{B} = 0 \ \text{ in } V \quad (8)$$
$$\mathbf{B} \cdot \hat{\mathbf{n}} = 0 \ \text{ on } \partial V \quad (9)$$

where V is a volume enclosed by a surface ∂V and $\hat{\mathbf{n}}$ is the unit vector normal to the surface.

The SPEC code can be used to calculate vacuum fields given a boundary magnetic surface. In fact, Eq. (7) can be seen as a Taylor state $\nabla \times \mathbf{B} = \mu\mathbf{B}$ with no parallel current, namely $\mu = 0$. These states can be computed with SPEC by considering one relaxed volume ($N = 1$) with no current ($\mu = 0$) and no pressure ($p = 0$), and providing the geometry of the boundary and the total enclosed toroidal flux. Equation (8) is satisfied by construction since the magnetic field in SPEC is given in terms of a magnetic vector potential, $\mathbf{B} = \nabla \times \mathbf{A}$. Equation (9) is also satisfied by construction since, on the boundary, the geometry of the coordinate grid coincides with the geometry of the boundary and the magnetic field on the boundary has only tangential components.
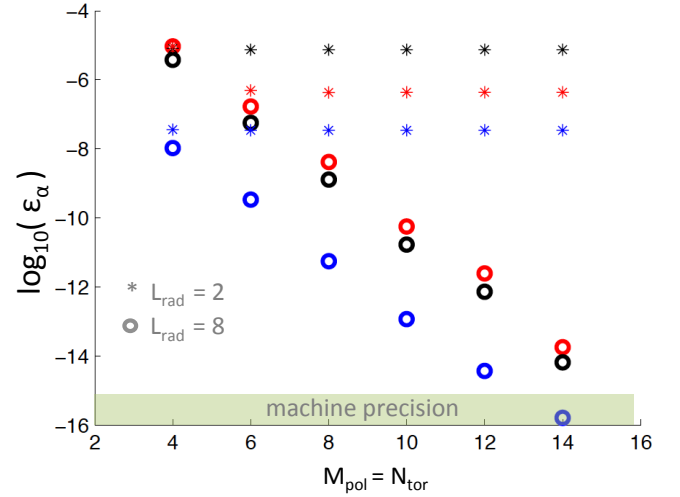

FIG. 1: Convergence of the error as a function of Fourier resolution, for the $l = 2$ stellarator case. Stars: $L_{rad} = 2$. Circles: $L_{rad} = 8$. The three components are shown in different colours (red: s, black: θ, blue: φ). Here the representation of the boundary is fixed with highest Fourier modes $m = n = 4$.
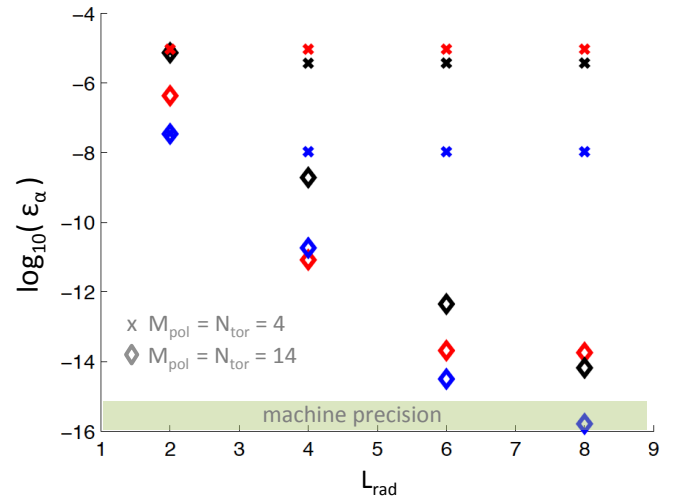

FIG. 2: Convergence of the error as a function of radial resolution, for the $l = 2$ stellarator case. Crosses: $M_{pol} = N_{tor} = 4$. Diamonds: $M_{pol} = N_{tor} = 14$. The three components are shown in different colours (red: s, black: θ, blue: φ). Here the representation of the boundary is fixed with highest Fourier modes $m = n = 4$.

Verification of SPEC therefore requires numerical proof that the SPEC solution satisfies Eq. (7) with increasing accuracy as numerical resolution is increased and with an error approaching machine precision for sufficiently high resolution.

Two stellarator configurations are considered: a classical $l = 2$ stellarator with 5 field periods [14] and a W7-X limiter configuration of the first experimental campaign [7]. The latter includes a large $n = 5/N_P$, $m = 6$, mag-
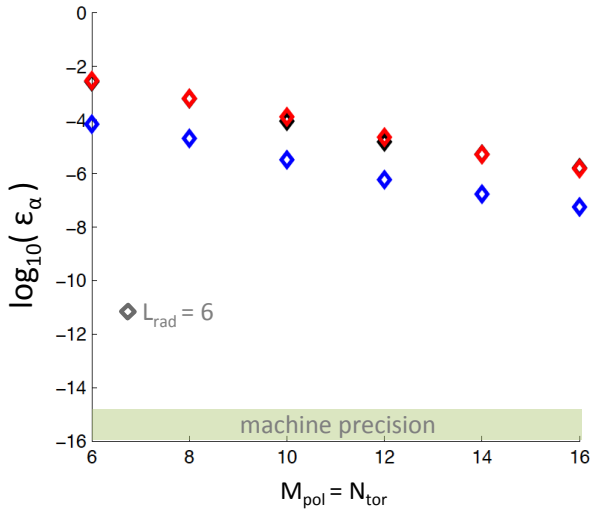
FIG. 3: Convergence of the error as a function of Fourier resolution, for the W7-X case. Here $L_{rad} = 6$. The three components are shown in different colours (red: s, black: θ, blue: φ). Here the representation of the boundary is fixed with highest Fourier modes $m = n = 6$.

netic island chain located inside the last closed flux surface, where the vacuum rotational transform is $\iota = 5/6$. For each configuration, a boundary can be provided to SPEC by extracting the geometry of a magnetic surface from the vacuum field calculated with a Biot-Savart solver. A description of the method used to extract the surface geometry from field-line-tracing on vacuum fields is presented in the Appendix A. Of course, an accurate description of the W7-X boundary requires more Fourier harmonics than that of the $l = 2$ stellarator boundary.

In order to quantify the error in SPEC we define the quantity

$$\varepsilon_\alpha = \frac{1}{V} \int ds \oint d\theta \oint d\varphi \; \mathcal{J}(s,\theta,\varphi) |(\nabla \times \mathbf{B} - \mu\mathbf{B}) \cdot \nabla\alpha| \tag{10}$$

where $\alpha = s, \theta, \varphi$ and $V = \int ds \oint d\theta \oint d\varphi \; \mathcal{J}(s,\theta,\varphi)$ is the total volume. The value of ε_α measures the volume-averaged distance from the exact solution, component by component. Figure 1 shows, for the $l = 2$ stellarator case, the convergence of ϵ_α towards machine precision (10^{-16}) as the Fourier resolution is increased at fixed high radial resolution. The convergence is exponential, $\varepsilon_\alpha(M_{pol}) \sim 10^{-\kappa M_{pol}}$, with $\kappa \approx 0.8$. Notice that for $L_{rad} = 2$ the error is dominated by the low radial resolution and thus no convergence is observed as the Fourier resolution is increased. Similarly, Fig. 2 shows that, at high Fourier resolution, the error converges towards machine precision as the radial resolution is increased. The convergence is also exponential, $\varepsilon_\alpha(L_{rad}) \sim 10^{-\kappa L_{rad}}$, with $\kappa \approx 2$.

The same exercise has been carried out for the W7-X vacuum field. As an example, Fig. 3 shows the corresponding error as a function of Fourier resolution, showing slower ($\varepsilon_\alpha \sim 10^{-\kappa M_{pol}}$, $\kappa \approx 0.33$) but clear conver-

gence. In fact, the Fourier resolution required to get the error down to machine precision is much higher because of the higher Fourier content of the boundary and the lower aspect ratio ($R/a \sim 10$ for W7-X and $R/a \sim 25$ for the $l = 2$ stellarator), which enhances the toroidicity effects and thus the Fourier content in the solution.

This verification exercise provides evidence that the SPEC code is calculating correctly, namely, with arbitrary accuracy, the solution to the equations it claims to be solving. It also motivates improvement in the numerics in order to make high Fourier resolution calculations converge faster towards the exact solution. We would like to remark, however, that our definition of the error, Eq. (10), is more stringent than one would need for verification purposes: instead of requiring $\mathbf{B}$ to be accurate, we require $\nabla \times \mathbf{B}$ to be accurate. Thus SPEC may be even more accurate than what this exercise shows. This may also be a reason why reaching high accuracy requires a higher Fourier resolution in the case of W7-X.

IV. COMPARISON TO BIOT-SAVART FIELDS

Beyond verification and with a view to progressing towards validation, it is interesting to investigate whether fixed-boundary vacuum field SPEC calculations can reproduce the solution to Biot-Savart calculations for the corresponding coil currents.

We start by comparing Poincaré plots obtained from field-line-tracing using both magnetic field solutions for a given set of initial positions. Figures 4 and 5 show the result of this comparison for both the $l = 2$ and the W7-X stellarator configurations, respectively. The corresponding vacuum rotational transform profiles are also shown in Figs. 6 and 7. Qualitatively, the agreement is excellent.

In order to better quantify the level of agreement between SPEC and Biot-Savart vacuum field solutions, we consider the magnetic field amplitude, $B = ||\mathbf{B}||$, which is a scalar field (thus independent of coordinates) and does not require post-processing analysis such as, for example, field-line-tracing (thus avoiding additional numerical errors). Even though the SPEC solution is given in terms of the vector potential, the magnetic field $\mathbf{B} = \nabla \times \mathbf{A}$ and its amplitude can be calculated *exactly* from the values of $\mathbf{A}$. As an example, Fig. 8 shows B on the boundary magnetic surface and on three different cross-sections, as obtained from the SPEC solution.

We define a metric for quantifying the level of agreement between SPEC and the corresponding Biot-Savart calculations:

$$\chi(R, Z, \varphi) = \frac{|B^*_{\text{SPEC}}(R, Z, \varphi) - B_{\text{BS}}(R, Z, \varphi)|}{B_{\text{BS}}(R, Z, \varphi)} \tag{11}$$

where $B^*_{\text{SPEC}} = (\Psi_{\text{BS}}/\Psi_{\text{SPEC}})B_{\text{SPEC}}$, and Ψ_{BS} and Ψ_{SPEC} are the total enclosed toroidal fluxes in each calculation. This normalization factor reflects the fact that in a fixed-boundary equilibrium calculation the total enclosed
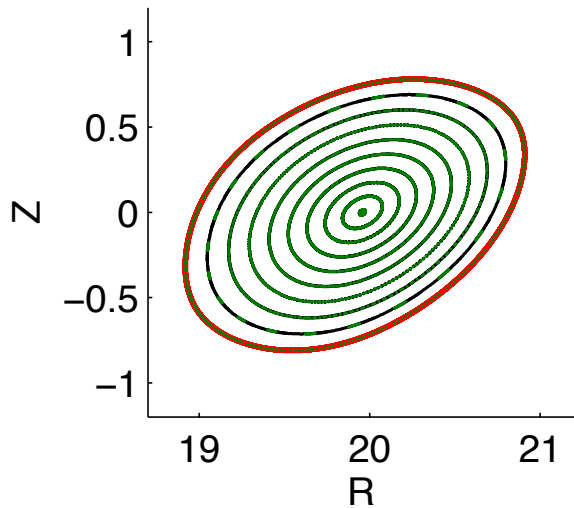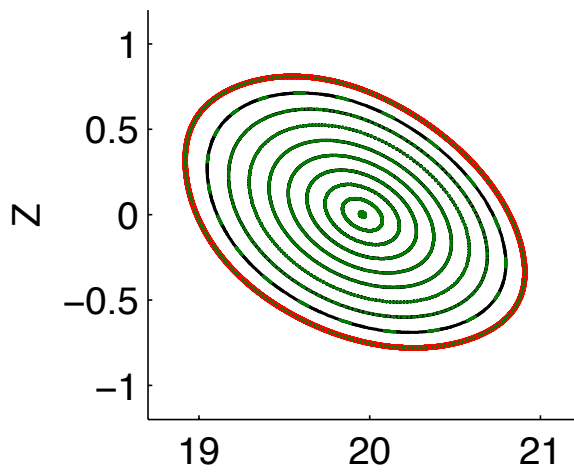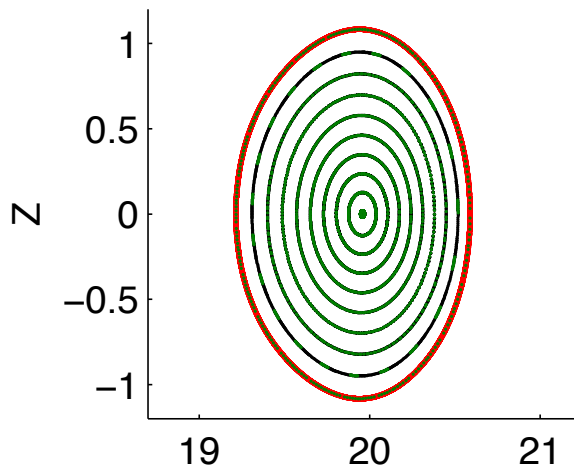
FIG. 4: Poincaré plot of the vacuum field for an $l = 2$ stellarator. Three cross-sections are shown: $\varphi = 0°$ (top), $\varphi = 24°$ (middle), and $\varphi = 48°$ (bottom). Results obtained using both the SPEC (black) and Biot-Savart (green) solutions. The boundary provided to SPEC is also indicated (solid red line). The representation of the boundary has Fourier modes as high as $m = n = 12$.
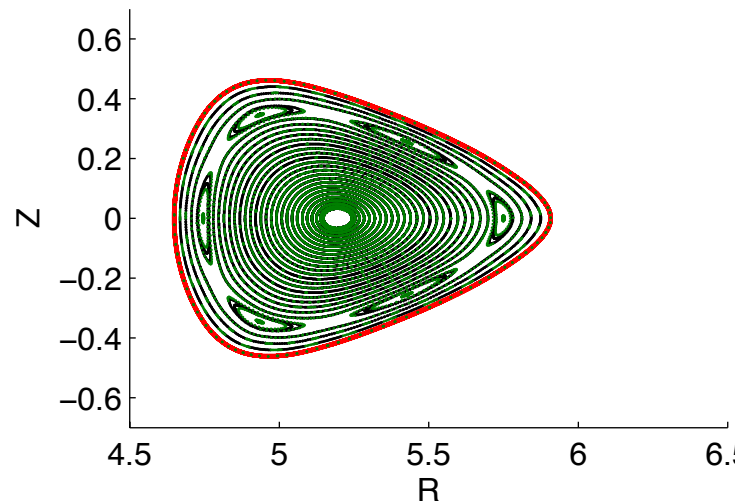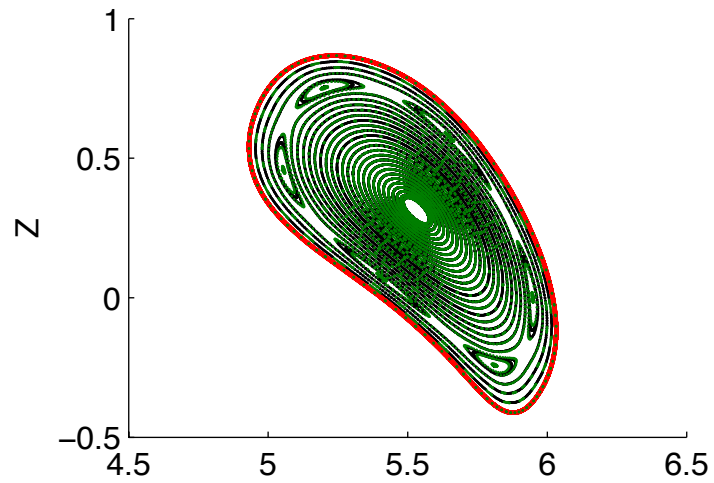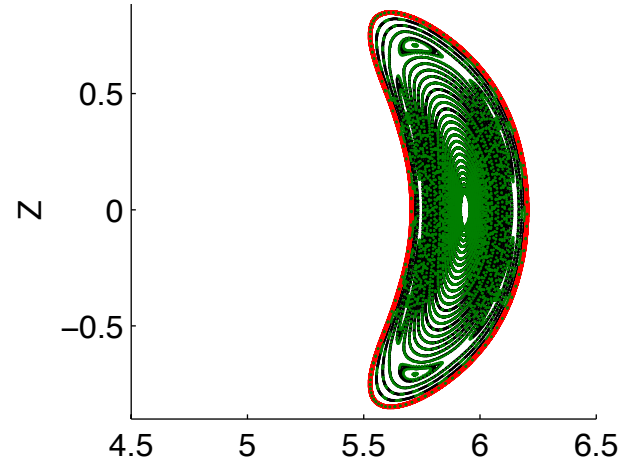
FIG. 5: Poincaré plot of the vacuum field for the W7-X case. Three cross-sections are shown: $\varphi = 0°$ (top), $\varphi = 18°$ (middle), and $\varphi = 36°$ (bottom). Results obtained using both the SPEC (black) and Biot-Savart (green) solutions. The boundary provided to SPEC is also indicated (solid red line). The representation of the boundary has Fourier modes as high as $m = n = 12$.
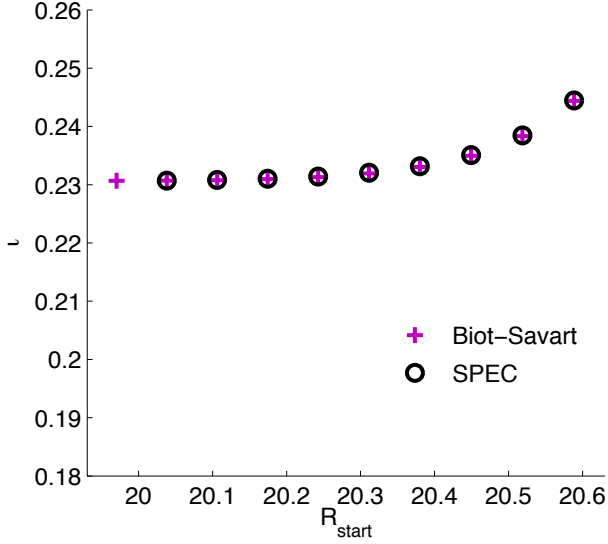
FIG. 6: Rotational transform profile in the $l = 2$ stellarator configuration as given by SPEC (circles) and from the Biot-Savart solution (crosses), obtained by tracing field lines initially at $(R_{start}, Z = 0)$.
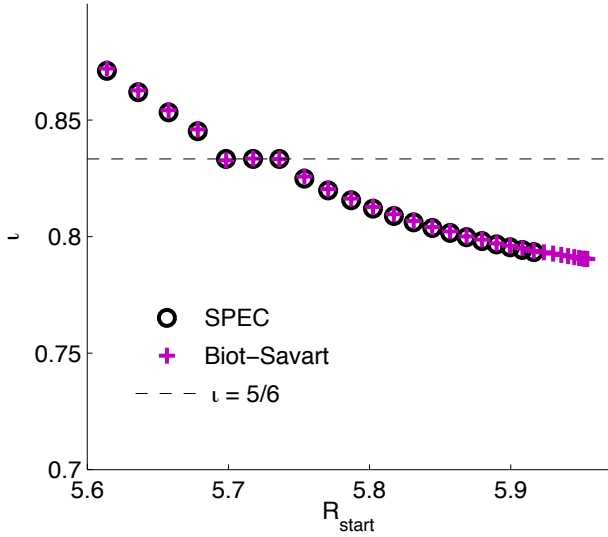

FIG. 7: Rotational transform profile in the W7-X configuration as given by SPEC (circles) and from the Biot-Savart solution (crosses), obtained by tracing field lines initially at (R_{start}, Z_{start}) such that the O-point of the island chain is crossed.
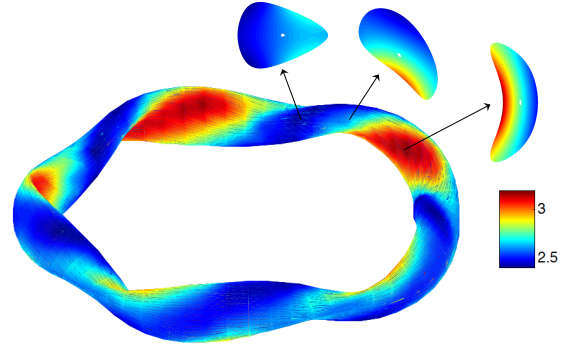

FIG. 8: Amplitude of the magnetic field on the boundary magnetic surface and on three different cross-sections. Results obtained from SPEC calculations of the W7-X vacuum field.
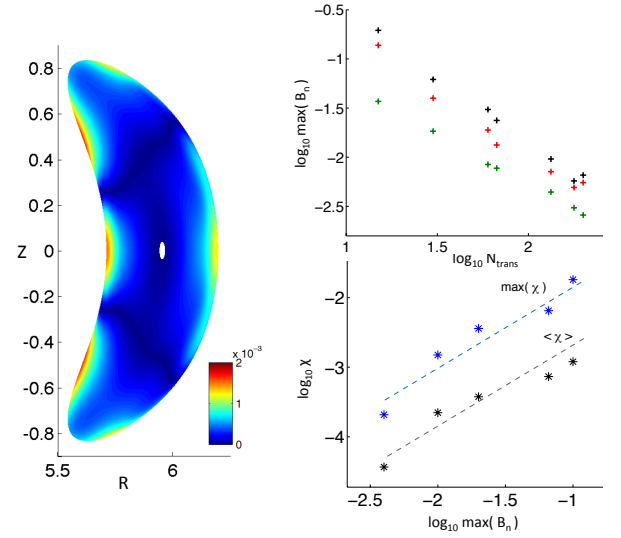

FIG. 9: Distance χ between SPEC and Biot-Savart solutions for the W7-X vacuum field. Left: $\chi(R, Z)$ on the bean cross-section. Top right: B_n as a function of the number of toroidal transits used for the boundary extraction (different colors are for different surfaces with different ι). Bottom right: maximum and volume-average of $\chi(R, Z, \varphi)$ as a function of B_n. Dashed lines have slope 1.

toroidal flux is irrelevant and only acts as a global scale-factor on the magnetic field strength.

Figure 9 (left panel) shows the value of χ for the W7-X case on the $\varphi = 0$ cross-section. The values of χ range from $\chi \approx 4 \times 10^{-9}$ in the core to $\chi \approx 1.6 \times 10^{-3}$ close to the boundary. Very similar values are obtained for the $l = 2$ stellarator case (data not shown). That means that the SPEC and Biot-Savart solutions agree within 0.1%, with very good agreement far from the boundary.

An increase in the numerical resolution used in either SPEC or the Biot-Savart solver does not produce substantially lower values of χ (data not shown). This suggests that the distance between the two calculations is due to some difference in the boundary representation. In fact, while SPEC assumes the existence of *one* flux-surface (the boundary), the Biot-Savart calculation does not. Since the boundary geometry in SPEC is extracted from field-line-tracing of the Biot-Savart solution, it is possible that (1) the extraction is not precise enough, or (2) there is no *exact* magnetic surface traced by a field-line. These possibilities can be investigated by measuring the quantity $B_n \equiv \mathbf{B}_{BS} \cdot \hat{\mathbf{n}}$, where $\hat{\mathbf{n}}$ is the unit vector

normal to the extracted boundary and $\mathbf{B}_{\mathrm{BS}}$ is the Biot-Savart solution used for the extraction. Figure 9 (top right panel) shows that B_n is non-zero but can be reduced by increasing the number of toroidal transits used to generate points on the surface. We expect that the distance between SPEC and Biot-Savart solutions, χ, monotonically decreases when reducing B_n, with a dependence that can be estimated as follows. Let us assume that the toroidal flux is roughly $\psi \sim B\pi a^2 \sim const$, where a is the effective radius of the cross-section. Thus the error in the magnetic field magnitude, δB, produced by an error in the boundary geometry, δa, is $\delta B/B \sim 2\delta a/a$. Since we expect $\delta a \sim B_n$, we conclude that the distance between the two solutions, χ, should scale linearly with B_n. Figure 9 (bottom right panel) confirms this dependence.

In this Section, we have demonstrated how we can use SPEC in fixed-boundary mode to recover the experimental state of W7-X (at least for a vacuum). This is an important first step towards experimental equilibrium reconstruction activities using SPEC.

V. VERIFICATION OF PLASMA EQUILIBRIA

A complete verification of the SPEC code requires performing equilibrium calculations with $N > 1$, so that the algorithm solving the force-balance equation, Eq. (2), is also tested. To this aim, we consider the $l = 2$ stellarator described in Sec. III with $N = 2$ relaxed volumes separated by an ideal interface. As input parameters, one must provide (i) the boundary geometry; (ii) the pressures, p_1 and p_2, and the enclosed toroidal fluxes, ψ_1 and ψ_2, in each relaxed volume; (iii) and three additional numbers, e.g., the rotational transform on each side of the inner interface, ι^+ and ι^-, and the edge rotational transform, ι_a. The solution for the equilibrium consists of the geometry of the internal interface and the magnetic field in each relaxed volume. An example of such equilibrium is shown in Fig. 10, with the internal interface geometry as well as a Poincaré plot of the magnetic field in each volume. The rotational transform at the edge has been chosen to be equal to the vacuum edge transform, $\iota_a \approx 0.243$ (see Fig. 6). The rotational transform on the internal interface has been chosen to be continuous and equal to a noble irrational, $\iota^+ = \iota^- = (n_1 + \gamma n_2)/(m_1 + \gamma m_2) \approx 0.2309$, guided by the KAM theorem [15] and the work of Greene [16], which show that the most robust surfaces are those with most irrational transform. Here $\gamma = (1 + \sqrt{5})/2$ is the golden mean and $n_1/m_1 = 23/100$ and $n_2/m_2 = 231/1000$. Finally, the pressures and enclosed toroidal fluxes are $p_1 = p_2 = 0$ and $\psi_1 = 0.25 = 1 - \psi_2$.

Verification of SPEC demands numerical proof that Eqs. (1) and (2) are satisfied to arbitrary precision for sufficiently high resolution. As before, we use Eq. (10) to quantify the error in the Beltrami field in each volume. For a measure of the force *imbalance* on the internal in-
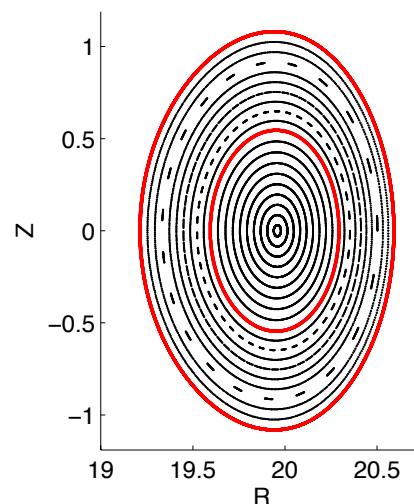

FIG. 10: Poincaré plot ($\varphi = 0°$) of the SPEC magnetic field for an $l = 2$ stellarator equilibrium with 2 volumes. The boundary provided to SPEC and the self-consistently calculated internal interface are also indicated (solid red lines).
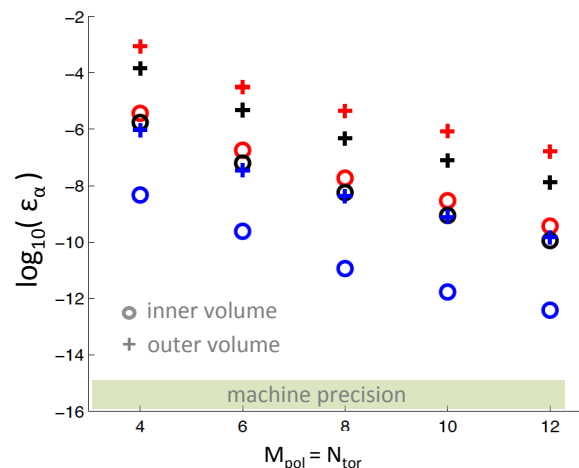

FIG. 11: Convergence of the error as a function of Fourier resolution, for the $l = 2$ stellarator case with $N = 2$ volumes. Circles: inner volume. Crosses: outer volume. The three components are shown in different colours (red: s, black: θ, blue: φ). Radial resolution is $L_{rad} = 6$ in both volumes.

terface, we define the quantity

$$|f| = \frac{1}{\mathcal{N}} \sum_{mn} [[p + \frac{B^2}{2}]]_{mn} \qquad (12)$$

where $\mathcal{N} = N_{tor} + 1 + M_{pol}(2N_{tor} + 1)$ is the total number of Fourier modes. In SPEC, a Newton method is used to iteratively find the zero of the force-balance equation.

Figure 11 shows convergence of the error in the Beltrami fields as a function of Fourier resolution. For each of these equilibria, we verify that $|f| \sim 10^{-16}$, i.e., force-balance is satisfied to machine precision in all cases.
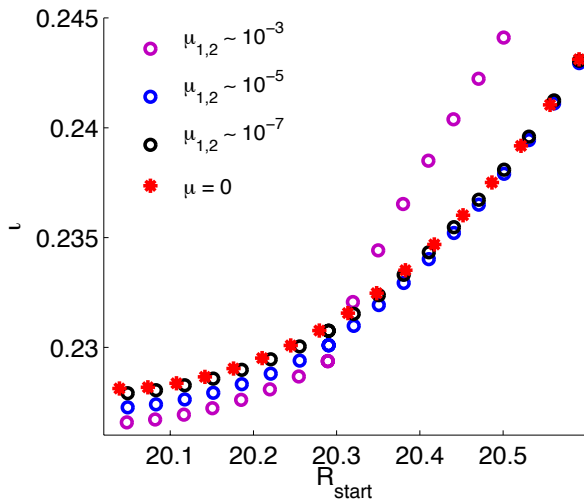
FIG. 12: Rotational transform profile for the $l = 2$ stellarator. Red stars: $N = 1$ volume in vacuum. Circles: $N = 2$ volumes with different values of $\mu_{1,2}$. Results obtained from field-line tracing on the different SPEC solutions.
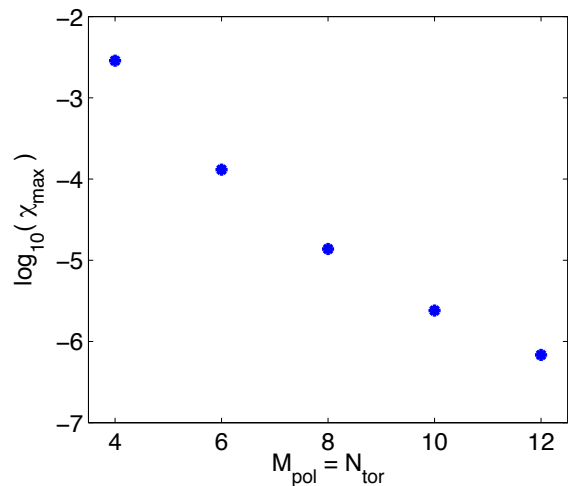

FIG. 13: Convergence of the maximum distance between the $N = 2$ and $N = 1$ solutions as a function of Fourier resolution, for the $l = 2$ stellarator case.

Since we have, for computational expediency, chosen to enforce the rotational transform constraint (to ensure that ι is continuous), the values of μ_1 and μ_2 are, in general, non-zero. This implies that there is current in the plasma and therefore the rotational transform profile differs from that of the vacuum (Figure 12). A state with $\mu_1 = \mu_2 = 0$ and with a continuous rotational-transform can be obtained by iterating on ψ_1 and ι_a. A Newton method was implemented to this aim. SPEC is run sequentially by iterating on (ψ_1, ι_a) in order to minimize $(|\mu_1|, |\mu_2|)$. In a few iterations, the values of $\mu_{1,2}$ can be made arbitrarily small and the corresponding rotational transform profile approaches the vacuum profile, as shown in Fig. 12. We can quantify the difference between the $N = 2$ solution and the $N = 1$ vacuum solution by using a metric, χ, as the one defined in Eq. (11). Even when $\mu_{1,2} \to 0$, the agreement between the two solutions is limited by the errors in the Beltrami fields which, as we have showed, can be reduced by increasing the Fourier resolution. Figure 13 shows that the distance between the $N = 2$ and $N = 1$ calculations converges exponentially to zero as the Fourier resolution is increased.

VI. CONCLUSIONS

In this article, we have presented the first calculations performed with the SPEC code in stellarator geometries. A rigorous verification of the SPEC code has been carried out for vacuum fields, along with a quantitative comparison to Biot-Savart solutions. A verification of SPEC for partially relaxed stellarator equilbiria has also been presented. In all cases, errors have been quantified. Finally, we have reconstructed a vacuum stellarator field iteratively, starting from a multi-region, finite current,

plasma equilibrium. This represents a first step towards the computation of general zero-current stellarator equilibria.

In summary, we conclude that the SPEC code solves Eqs. (1) and (2) in stellarator geometries with arbitrary accuracy as numerical resolution is increased. Accuracy is the first and most important feature of numerical codes and needs to be guaranteed. Next comes robustness and speed. From this verification exercise, we have learned that the SPEC algorithm may need to be improved in order to maintain speed at high resolutions, which are required for an accurate description of certain stellarator geometries such as that of Wendelstein 7-X.

Appendix A: Boundary extraction from Biot-Savart

Magnetic surface geometries can be extracted from vacuum fields in terms of Fourier coefficients, R_{mn} and Z_{mn}, that can be used to describe the boundary in SPEC, see Eqs. (3) and (4).

Firstly, the vacuum field is computed using the Biot-Savart solver VACFIELD [17] provided a set of coil currents. The cylindrical components of the vacuum field are stored on a cylindrical grid, (R, φ, Z). Secondly, points on a field line are collected with the field-line tracer GOURDON [18]. Next, on each plane, $\varphi = const$, the Poincaré points are ordered for increasing poloidal magnetic angle θ. Fourier decompositions of R and Z are determined from the set of points obtained from the field line by ordering poloidally and toroidally.

The convergence properties of this procedure were studied by using a one-parametric sequence of resolution parameters, $N_R = N_\varphi = N_Z = 4.8\, N_{transit}$, and simultaneously increasing the size of the R and Z Fourier tables from $m_0 = n_0 = 12$ to 18. The maximum value of the normal component of the magnetic field on the approximation of the surface spanned by the field line, $\max |\mathbf{B}_0 \cdot \mathbf{n}|$, is used as figure of merit, vanishing for an ideal magnetic surface. The results of this convergence study are shown in Sec. IV.

[1] P. W. Terry, M. Greenwald, J.-N. Leboeuf, G. R. McKee, D. R. Mikkelsen, W. M. Nevins, D. E. Newman, and D. P. Stotler. Validation in fusion research: Towards guidelines and best practices. *Physics of Plasmas*, 15(6):062503, 2008.

[2] R. B. White. *The Theory of Toroidally Confined Plasmas*. Imperial College Press, 2014.

[3] S. R. Hudson, R. L. Dewar, G. Dennis, M. J. Hole, M. McGann, G. von Nessi, and S. Lazerson. Computation of multi-region relaxed magnetohydrodynamic equilibria. *Physics of Plasmas*, 19(11):112502, 2012.

[4] J. Loizu, S. Hudson, A. Bhattacharjee, and P. Helander. Magnetic islands and singular currents at rational surfaces in three-dimensional magnetohydrodynamic equilibria. *Physics of Plasmas*, 22(2):022501, February 2015.

[5] J. Loizu, S. R. Hudson, a. Bhattacharjee, S. Lazerson, and P. Helander. Existence of three-dimensional ideal-magnetohydrodynamic equilibria with current sheets. *Physics of Plasmas*, 22(9):090704, September 2015.

[6] J. Loizu, S. R. Hudson, P. Helander, S. A. Lazerson, and A. Bhattacharjee. Pressure-driven amplification and penetration of resonant magnetic perturbations. *Physics of Plasmas*, 23(5):055703, May 2016.

[7] T. Sunn Pedersen, T. Andreeva, H.-S. Bosch, S. Bozhenkov, F. Effenberg, M. Endler, Y. Feng, D.a. Gates, J. Geiger, D. Hartmann, H. Hölbe, M. Jakubowski, R. König, H.P. Laqua, S. Lazerson, M. Otte, M. Preynas, O. Schmitz, T. Stange, and Y. Turkin. Plans for the first plasma operation of Wendelstein 7-X. *Nuclear Fusion*, 55(12):126001, November 2015.

[8] M.J Hole, S.R Hudson, and R.L Dewar. Equilibria and stability in partially relaxed plasmavacuum systems. *Nuclear Fusion*, 47(8):746–753, August 2007.

[9] S. R. Hudson, M. J. Hole, and R. L. Dewar. Eigenvalue problems for Beltrami fields arising in a three-dimensional toroidal magnetohydrodynamic equilibrium problem. *Physics of Plasmas*, 14(5):052505, 2007.

[10] G. R. Dennis, S. R. Hudson, R. L. Dewar, and M. J. Hole. The infinite interface limit of multiple-region relaxed magnetohydrodynamics. *Physics of Plasmas*, 20(3):032509, 2013.

[11] J. B. Taylor. Relaxation of Toroidal Plasma and Generation of Reverse Magnetic Fields. *Physical Review Letters*, 33(19):1139–1141, November 1974.

[12] Milton Abramowitz and Irene A Stegun. *Handbook of Mathematics*. Dover Publications, 1965.

[13] A. A. Blank, K. O. Friedrichs, and H. Grad. Theory of Maxwell's equations without displacement current. Technical report, Courant Institute of Mathematical Sciences, New York University, 1957.

[14] Jeffrey P. Freidberg. *Ideal MHD*. Cambridge University Press, 2014.

[15] J. D. Meiss. Symplectic maps, variational principles, and transport. *Reviews of Modern Physics*, 64(3):795–848, July 1992.

[16] John M. Greene. A method for determining a stochastic transition. *Journal of Mathematical Physics*, 20(6):1183, 1979.

[17] E. Strumberger and E. Schwarz. IPP Report 5/112, MPI Plasmaphysik, Garching, Germany. http://hdl.handle.net/11858/00-001M-0000-0027-16A7-C. Technical report, 2005.

[18] G. Gourdon, D. Marty, E.K. Maschke, and J.D. Dumont. Configurations du type stellarator avec puits moyen et cisaillement des lignes magnétiques. *Proceedings of the 3rd International Conference on Plasma Physics Controlled Nuclear Fusion Research, Novosibirsk, USSR, 1968, Nucl. Fusion Suppl.*, 1:847, 1969.